Semiconductor Quantum-Dot Nanostructures: Their Application in a New Class of Infrared Photodetectors

Elias Towe and Dong Pan

Invited Paper

***Abstract*—Semiconductor quantum-dot nanostructures are interesting objects for fundamental as well as practical reasons. Fundamentally, they can form the basis of systems in which to study the quantum mechanics of electrons confined in zero-dimensional (0-D) space. In practice, the dots can be embedded in the active regions of a new class of electronic and optoelectronic devices with novel functionalities. This paper reviews the state-of-the-art in the use of these objects in infrared detectors. It describes the progress, challenges, and projections for continued development of normal-incidence intersublevel detectors operating in the spectral region between 6 and 20 μm.**

***Index Terms*—Intersublevel infrared photodetectors, nanostructures, normal-incidence detectors, quantum dots, self-assembled dots, zero-dimensional space.**

I. Introduction

FOR OVER three decades, most applications of photonics and optoelectronics have been confined between the visible and near-infrared range of the optical spectrum (0.4 to 2.0 μm). The most common applications in this regard include long-distance fiberoptic communications, short-distance local-area interconnections for information and data processing systems, data storage servers, optical sensing, and imaging. Recently, however, advances in the synthesis of semiconductor materials, together with innovative device design concepts, are beginning to enable the realization of optical devices in the ultraviolet (100–400 nm) and the infrared (2–20 μm) ranges of the optical spectrum. These advances are expected to open use up of these portions of the spectrum for new and exciting applications. The development of nitride-based III–V semiconductors, for instance, is expected to bring forth a new class of optical sources [1] and detectors [2] in the blue and ultraviolet ranges of the spectrum. At the same time, innovations in device design concepts and the artificial restructuring of semiconductor materials are resulting in a new class of sources and detectors in the infrared; the most advanced of these devices include the unipolar quantum cascade laser [3] and the intersubband infrared detector [4]. This progress portends the beginnings of practical nanostructure science and engineering.

Manuscript received November 12, 1999; revised March 27, 2000. This work was supported by the Army Research Office, Research Triangle, NC, under Grant DAAG55-97-1-0006, and is monitored by Dr. M. Dutta.

The authors are with the Laboratory for Optics and Quantum Electronics, University of Virginia, Charlottesville, VA 22903-2442 USA (e-mail: towe@virginia.edu; dp7u@virginia.edu).

Publisher Item Identifier S 1077-260X(00)05098-X.

II. Background on Infrared Radiation

This paper discusses the use of semiconductor nanostructures in the detection of infrared radiation. We begin with a brief discussion of infrared radiation for a perspective. Infrared radiation is a form of electromagnetic energy covering a specific band of the electromagnetic spectrum. This band is generally taken to be from about 0.7 to about 1000 μm. Most objects emit electromagnetic radiation that can be described by Planck's radiation law [5], which can be written in the form

$$\frac{\partial\varphi(T,\lambda)}{\partial\lambda} = \frac{2\pi c}{\lambda^4[\exp(hc/\lambda kT)-1]} \text{ photons}/(\text{cm}^2\cdot\text{s}\cdot\mu\text{m})$$

where

$\partial\varphi(T,\lambda)/\partial\lambda$	spectral exitance, defined as the number of photons emitted per second, per unit area, per wavelength (in microns);
c	velocity of light;
h	Planck's constant;
k	Boltzmann's constant; and
T	absolute temperature of the emitting body.

This law was postulated for a *blackbody*—defined as an object that emits or absorbs radiation of all wavelengths. The ideas put forth by Planck and his contemporaries in the early 1900s on the challenge of understanding the physical meaning of this law are often considered to be the beginning of modern quantum theory.

A plot of the spectral exitance, $\partial\varphi(T,\lambda)/\partial\lambda$, as a function of both wavelength and absolute temperature is very instructive. Such as plot is shown in Fig. 1. The spectral exitance is more commonly expressed as the radiant power per unit area per wavelength. We have expressed the spectral exitance in terms of photons per square centimeter, per second, per wavelength (in microns) to make the main point of our discussion clear. Several useful observations can be made from Fig. 1; the most important are the following: increasing the temperature of a blackbody decreases the wavelength at which the maximum number of photons is emitted; the hotter a blackbody is, the more photons it emits; quite a large number of photons ($>10^{15}$ photons/[$\text{cm}^2\cdot\text{sec}\cdot\mu$m]) are emitted by bodies whose temperatures are between 100 and 300 K. The significance of this temperature range is that even without any deliberate heating, most objects emit a large number of infrared photons. The spectral

1077–260X/00$10.00 © 2000 IEEE

Authorized licensed use limited to: IEEE Xplore. Downloaded on November 14, 2008 at 07:29 from IEEE Xplore. Restrictions apply.

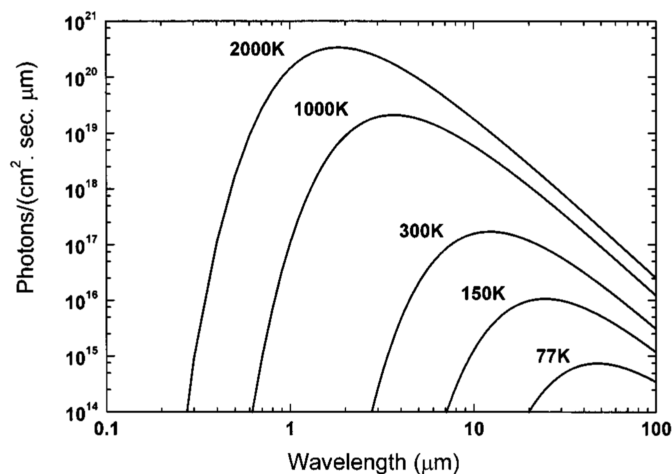

Fig. 1. The spectral excitance, showing the rate of emission of infrared photons per unit area, per wavelength, by a blackbody at various temperatures, calculated using Planck's radiation law for blackbodies.

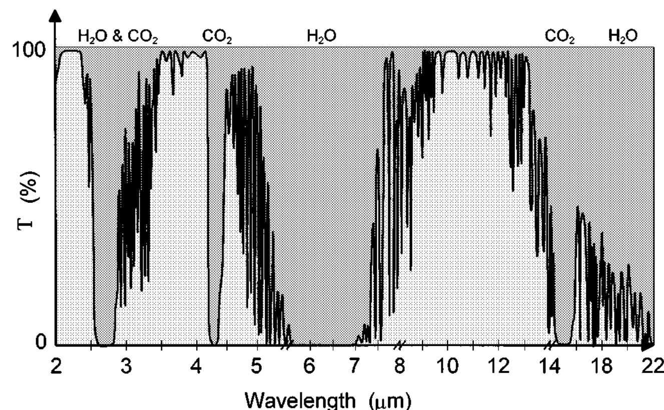

Fig. 2. Atmospheric transmission windows in the infrared range of the optical spectrum. This example of the spectrum is for transmission through 300 m of humid air at sea level (this figure is courtesy of Drs. Federico Capasso and Claire Gmachl of Bell Laboratories, Lucent Technologies, Murray Hill, NJ).

bandwidth defined by the photons in this temperature range begins from a little over 3 μm to about 70 μm. The practical implication of this is that even in the dark (when human vision is lacking), objects that are extremely cold can be "seen" by detecting the copious infrared photons emitted. The sensed photons can be made to render the object "visible" by clever transduction schemes.

In order to determine the appropriate spectral band that is useful for general sensing and vision applications in the infrared, one must take into account the interaction of the radiation emitted by a given body with the atmosphere. This is because some atmospheric gases have molecular resonances within the infrared spectral band. These gases, notably carbon dioxide and water vapor, act as absorbing centers that render some wavelengths of the infrared unusable. The spectrum in Fig. 2 shows the transmission windows found in 300 m of humid air at sea level. From Planck's radiation curves of Fig. 1, and the atmospheric transmission windows of Fig. 2, we see that radiant emission from objects at ambient temperature (300 K) will pass through the atmosphere in the 3–5-μm band and also in the 8–14-μm band. These windows are the infrared spectral bands that are useful for most terrestrial applications.

III. INFRARED DETECTORS

No single detector is available for sensing over the entire range of the infrared spectrum. Available detectors fall into one of two broad families: either the thermal family of detectors or the photon (quantum) family of detectors. Within the traditional photon family of detectors, the devices are either fabricated from an intrinsic or an extrinsic semiconductor. Thermal detectors operate by converting infrared radiation into heat; this changes the temperature of the detector material to induce some measurable change in a material property. In this review, we are only interested in photon detectors and will not discuss thermal detectors any further. Photon detectors, usually referred to simply as photodetectors, operate by the absorption of photons by electrons bound in a crystalline lattice of atoms. The energy of the photons excites electrons into higher (conduction band) energy

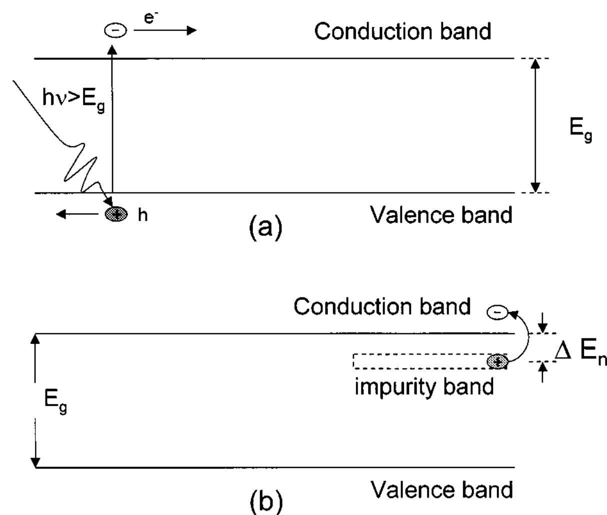

Fig. 3. Schematic energy band diagrams for the basic operation of (a) an intrinsic and (b) an extrinsic photodetector.

states. With appropriate potential bias, the photoelectrons can be collected as current and the presence of the infrared photons is thus registered.

A. *Intrinsic Infrared Detectors*

The basic operation of the intrinsic detector is illustrated in the energy band diagram of Fig. 3(a). An electron in the valence band absorbs a photon, $h\nu$, whose energy is slightly larger than the intrinsic band gap, E_g. The absorbed photons excite electrons into the conduction band of the semiconductor where the photoelectrons are collected as current. The detection of photons incident onto a semiconductor, therefore, depends on the relationship of the semiconductor's band gap to the energy of the photons. For the most part, the band gap of the most common infrared semiconductors [6]–[8], such as (Hg,Cd)Te or (Pb,Sn)Te, can be tailored to suit the particular infrared wavelength to be sensed. For these materials, the band gaps are generally tuned by selecting the appropriate composition of Hg and Cd in the (Hg,Cd)Te materials system, or Pb and Sn in the (Pb,Sn)Te materials system. The detection of infrared wavelengths from 3 to

Authorized licensed use limited to: IEEE Xplore. Downloaded on November 14, 2008 at 07:29 from IEEE Xplore. Restrictions apply.

15 μm, for example, would require the tuning of the band gap from 413.3 to 82.7 meV. Although it is possible to synthesize these materials with compositions that correspond to these band gaps, several drawbacks make this task difficult. One of the difficulties is that materials with such narrow band gaps tend to be soft—a property attributed to weak interatomic bonds. The softness of the materials makes it difficult to grow and process large area wafers. Another problem is the difficulty of obtaining exact, desirable compositions for particular wavelengths.

B. Extrinsic Infrared Detectors

An extrinsic photodetector can usually be fabricated from a semiconductor such as silicon, doped with appropriate impurity atoms [9]. For silicon, the most common impurity atoms are arsenic atoms. The dopant impurity levels (which can broaden into bands) are generally located within the band gap; in the case of arsenic-doped silicon, the impurity band is located right below the conduction band, as shown in Fig. 3(b). An incident infrared photon with energy slightly larger than the difference between the conduction band edge and the top of the impurity band can excite a bound electron into the conduction band. Electrons excited from the impurity band into the conduction band in this manner can be collected as photoelectrons and, thus, current. Extrinsic photodetectors that operate under this principle are only sensitive in a rather narrow range of wavelengths. The wavelength range is usually limited by the combination of the semiconductor and its associated impurity atoms.

C. Quantum-Well Infrared Detectors

Intersubband photodetectors are a relatively recent innovation [4], [10]–[21]. The principle of their operation is intimately linked to quantum mechanics. The idea of using artificially structured semiconductors with quantum wells in them for photodetection was first proposed by Esaki and Sakaki [22]. It is illustrated in its most basic form in Fig. 4. Although the illustration shows both conduction and valence band quantum wells, intersubband photodetectors are usually implemented as single (unipolar) carrier devices. Consider tthe conduction band quantum well in the GaAs–(Al,Ga)As materials system as an example: for extremely high potential barriers and parabolic bands, the textbook approach for calculating the eigenstates in a rectangular well potential can be used to obtain the energy levels in the well as

$$E_n = \frac{\hbar^2 \pi^2}{2m^* L_w^2} n^2$$

where

- m^* effective mass of an electron;
- L_w width of the quantum well; and
- n integer.

The other parameters have their usual meanings. A transition that could lead to photodetection in a quantum well can occur between the ground state and the first excited state, within the same band—i.e., an intersubband transition. Quantum-well structures are usually designed with at least two confined states in them or one confined state and a quasi-continuum or an extended state above the well. If the structure has only two confined states in it, say the ground state and the first excited state, then the energy separation between them (in the simple rectangular model of the conduction band quantum well) is

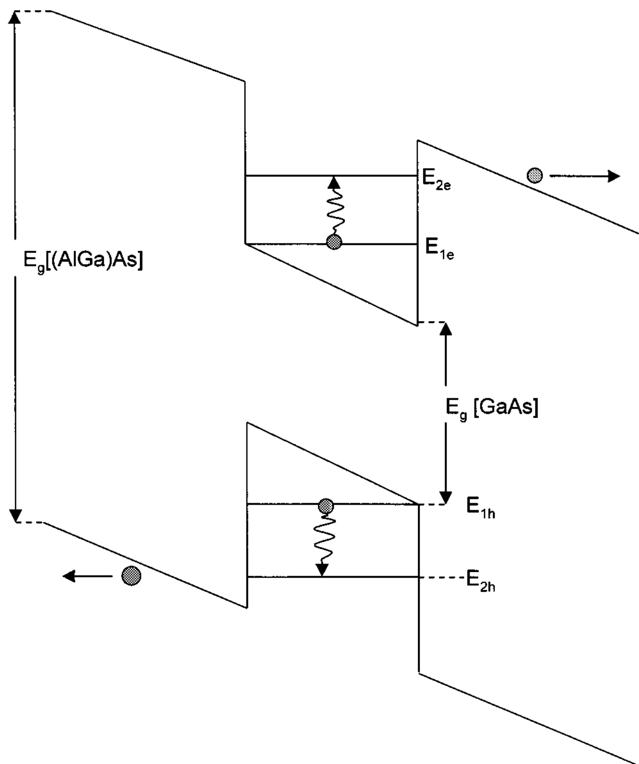

Fig. 4. Schematic energy band diagram of the quantum-well infrared photodetector. The transitions that result in photodetection occur either within the conduction band alone or within the valence band alone; in other words, these are intersubband transitions.

$$\Delta E = E_2 - E_1 = \frac{3\hbar^2 \pi^2}{2m^* L_w^2}.$$

An incident infrared photon with energy slightly larger than the intersubband spacing of the quantized states in the well can promote the ground-state electron to the excited state, where, with appropriate bias, it can tunnel out of the well or is excited into the quasi-continuum state and then collected as a photoelectron. The first conduction band quantum-well structure to operate as a detector was reported by Levine *et al.* [11]. Numerous implementations of the basic quantum-well infrared photodetector (QWIP) have since been reported by many authors [4], [10]–[21]; see the reviews in [4], [12], and [13], for example. This type of detector, however, has some disadvantages: among them are a lower quantum efficiency and a lower responsivity than is generally found in conventional bulk detectors fabricated from a direct gap semiconductor such as (Hg,Te)Cd. Furthermore, the QWIP is insensitive to normally incident light because the intersubband transitions (that result in photodetection) are only allowed for light propagating in the plane of the quantum well; only in this case is the electric field vector of the incident light parallel to the direction of the current dipole of the confined charge. The insensitivity to normally incident light can be corrected by using a grating or a corrugated surface structure [18]–[21]. The grating or corrugation scatters a component of the normally incident light into the appropriate direction so that

Authorized licensed use limited to: IEEE Xplore. Downloaded on November 14, 2008 at 07:29 from IEEE Xplore. Restrictions apply.

its electric field vector is parallel to the current dipole, and it can thus be absorbed.

The two-dimensional (2-D) confinement of carriers in quantum wells—with the resultant discretization of the energy structure—is not the only approach to infrared photodetection. Carrier confinement in all three dimensions can also be used. This can be realized via semiconductor nanostructures known as quantum dots. Because the electronic wavefunctions are quantized in all three dimensions, the polarization selection rule for light absorption by dots favors absorption of light of all polarization directions. By definition, the lateral and vertical dimensions of a quantum dot are on the order of a de Broglie wavelength or the mean free path of an electronic carrier in the materials system in question. The beginning of the interest in quantum dot research can be traced back to a suggestion by Arakawa and Sakaki in 1982 [23] that the performance of semiconductor lasers could be improved by reducing the dimensionality of the active regions of these devices. Initial efforts at reducing the dimensionality of the active regions focused on using ultrafine lithography coupled with wet or dry chemical etching to form the three-dimensional (3-D) structures. It was soon realized, however, that this approach introduced defects that greatly limited the performance of such quantum-dot devices. Since the early 1980's, interest in epitaxially synthesizing quantum-dot structures has steadily grown. Initial efforts in this direction were mainly focused on the growth of (In,Ga)As nanometer-sized islands on GaAs substrates [24]–[28]. In 1992, the first epitaxial growth of defect-free quantum-dot nanostructures was achieved by using molecular beam epitaxy [27]. The realization that these defect-free structures are interesting for both fundamental as well as applied reasons has been at the root of the current spate of activity in quantum-dot work. Most of the practical quantum-dot structures today are synthesized by either molecular beam epitaxy [27] or metal organic chemical vapor deposition [28]. Practical optoelectronic devices, fabricated from quantum-dot structures, such as lasers [29]–[32] and photodetectors [33]–[39] have been reported. In this paper, we give a detailed discussion of the experimental development of a novel quantum-dot infrared photodetector.

IV. Self-Organized Quantum Dots

During the epitaxial synthesis of quantum dots, a film with a large in-plane lattice constant is grown on top of another with a smaller lattice constant. Under certain growth conditions, when the thickness of the film with the larger lattice constant exceeds a certain critical thickness, the compressive strain within the film is relieved by the formation of coherent islands. These islands maybe quantum dots. Coherent quantum-dot islands are generally formed only when the growth proceeds in what is known as the Stranski–Krastanow growth mode [40]. Dots grown under the Stranski–Krastanow growth mode can be defect free [27].

The formation of coherent quantum-dot islands via molecular beam epitaxy can usually be observed by an *in situ* reflection high-energy electron diffraction (RHEED) system. The onset of the transformation of the growth process from a 2-D layer-by-layer growth mode to a three-dimensional (3-D) island growth mode results in a spotty RHEED pattern. This is in contrast to the conventional streaky pattern generally observed for the layer-by-layer growth mode. The transition typically occurs after the deposition of a certain number of monolayers. For InAs on GaAs, this transition occurs after about 1.7 monolayers of InAs have been grown; this is the onset of islanding and, hence, quantum-dot formation. There have been extensive studies of island growth on other materials systems; these include (In,Ga,Al)As on InP [41], [42], InSb on GaSb [43], (In,Ga)As on Si [44], and Ge on Si [45]. Furthermore, there has also been work on the growth of quantum-dot nanostructures on substrates oriented in directions other than the [001] [46]–[48]. Growth on substrates with prefabricated templates and on vicinal substrates (slightly misoriented from a major crystal axis) has also been reported [49]–[52]. The different substrate orientations and materials combinations provide some degree of freedom in controlling the electronic structure (and, hence, the tunability of the infrared absorption wavelength) of the quantum dots. This is important because it is difficult, at present, to control the basic physical parameters of most self-organized quantum-dot nanostructures. The formation of the dots generally depends on the growth conditions—specifically, on such things as the substrate temperature and the flux of the constituent materials that control the amount of the deposited layer [53]. One of the major problems of self-organized quantum dots is that their size distribution is rather random; furthermore, the location of the dots in an array is very stochastic. This can be understood from a thermodynamic point of view if one considers the fact that the growth process is entropy driven. Unfortunately, the random size distribution has limited the potential performance of quantum-dot devices. In effect, the anticipated performance improvement of quantum-dot devices has not yet been realized. A simple manifestation of this problem is exemplified in the photoluminescence spectra of quantum dot samples. These spectra tend to be very broad. This is in spite of the fact that the expected linewidth from a single dot is extremely narrow [54]. These problems continue to engage a number of groups in research aimed at achieving uniform dot size and orderly spatial distribution.

Fig. 5 shows a typical photomicrograph of an (In,Ga)As-on-GaAs quantum-dot sample grown in our laboratory. This image was taken with an atomic force microscope (AFM). Atomic force microscopy and transmission electron microscopy are the tools generally used to measure the physical dimensions of the dots. When transmission electron microscopy is used, the effects of strain in the dots must be carefully taken into account because this type of microscopy can easily image strain fields. The nominal lateral extent of a dot grown in our laboratory is typically around 30–50 nm; the height can range from 5 to 12 nm. The shape of the dots depends on many factors; these include the growth conditions and the initial substrate surface. The shape of the dots can often be inferred from *in situ* RHEED studies [55] or from *ex situ* analysis of transmission electron microscope photomicrographs [56]. The most common dot shapes reported in the literature are pyramidal and plano-lens shapes. The

Authorized licensed use limited to: IEEE Xplore. Downloaded on November 14, 2008 at 07:29 from IEEE Xplore. Restrictions apply.

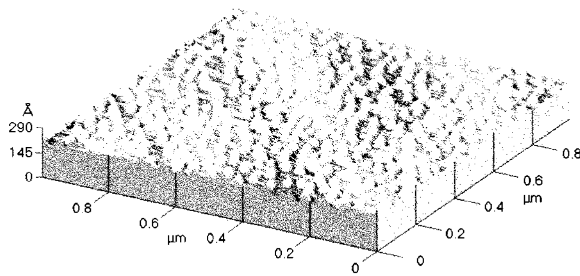

Fig. 5. An atomic force microscope photomicrograph of a typical self-organized (In,Ga)As-on-GaAs quantum-dot layer grown in our laboratory.

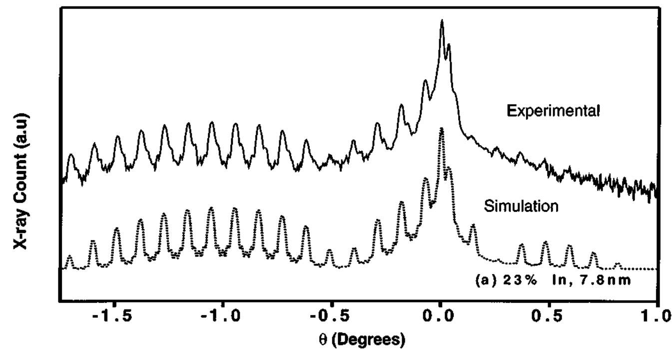

Fig. 6. High-resolution X-ray diffraction characterization of a five-period (In,Ga)As-on-GaAs quantum-dot superlattice with a nominal indium composition of 30%: the solid line shows the rocking-curve diffraction spectrum for the (004) reflection. The dashed line shows the analytically simulated spectrum. The indium composition extracted from the simulation is 23%, with an (In, Ga)as layer thickness of 7.8 Å.

shape of a dot plays an important role in determining the electronic structure.

The structural properties of quantum-dot superlattices are often characterized by using rocking-curve X-ray diffraction. In Fig. 6, we show a high-resolution X-ray diffraction rocking-curve for a five-period (In,Ga)As–GaAs quantum-dot superlattice with a nominal indium fraction of 30%. The solid curve was measured for the (004) reflection. We have also carried out measurements for other reflections [such as the (224) and the (113)]; similar results are obtained. Note that the experimental X-ray diffraction spectrum has up to 23 satellite peaks, with clear pendellösung fringes among the satellite peaks. This is evidence that the interfaces among the dot layers and the top cap layer are very sharp. The peak of the highest intensity, at 0°, is from the GaAs substrate. The strong asymmetry in the diffraction curve, with a shift toward the left, indicates the presence of compressive strain in the structure. A simulation of the experimental X-ray diffraction spectrum based on a solution of the Takagi–Taupin diffraction equations [57] is shown in the dashed curve in Fig. 6. The assumption made in the simulation is that the quantum-dot superlattice is similar to a tetragonally distorted (In,Ga)As–GaAs multiple quantum-well system. The structural parameters that yield a simulated curve that closely matches the experimental one are slightly different from the nominal values. The indium composition extracted from the simulation, for example, is about 23%; the calculated thickness of the (In,Ga)As layer is about 7.8 nm. The fact that this calculated thickness is larger

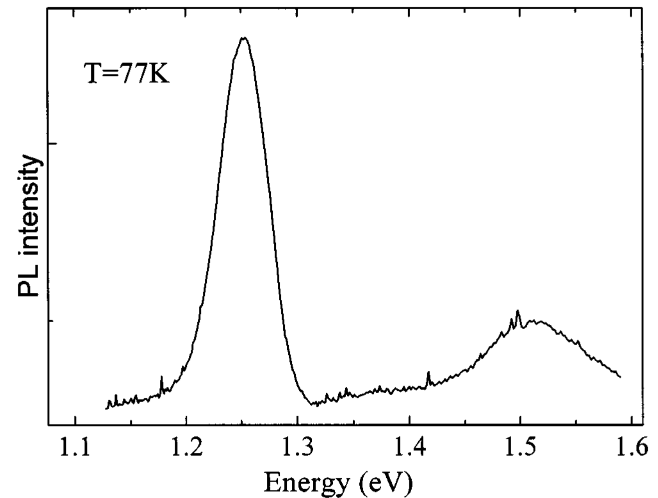

Fig. 7. A typical low-temperature (77 K) photoluminescence emission spectrum from one of our (In,Ga)As–GaAs self-organized quantum-dot structures; note that the intrinsic emission from the GaAs substrate (at ~1.5 eV) is also clearly observable.

than the nominal wetting layer of 3 nm implies that the dots do make a contribution to the X-ray signal. In fact, simulations based solely on the nominal thickness of the wetting layer do not match the experimental results. The lower calculated indium composition may indicate that after the onset of dot self-formation, the indium from the wetting layers diffuses into the dot structures. Results similar to these have been reported by others in the literature [58], [59].

The simplest optical characterization experiment that can be performed on quantum-dot structures is photoluminescence spectroscopy. The emission peak from such a structure is generally a good measure of the single-particle band gap of the dot. This is defined as the difference in energy for the transition of an electron from the lowest allowed conduction band level to the highest hole level in the valence band. For most experiments reported, the photoluminescence emission peak tends to be located between 1.1 and 1.2 eV. Fig. 7 shows a typical low-temperature (77 K) photoluminescence spectrum from one of our (In,Ga)As–GaAs quantum-dot superlattice structures. The emission from the quantum dots is located at about 1.25 eV. This emission energy is consistent with the average size of our dots. The peak located at about 1.5 eV is from the GaAs substrate. The spectral linewidth of the quantum-dot emission is about 50 meV; this is indicative of the wide dot size distribution. In practical dot ensembles, each dot may have a different size, shape, or strain distribution around it. The energy spectrum of each dot is therefore different. This means that under photoluminescence excitation, the emission spectrum will be inhomogeneously broadened. It is not surprising therefore to observe the broad spectral linewidth of the emission from some of our samples. We have also grown samples that exhibit photoluminescence emission linewidths that are narrower than 25 meV. We would like to point out that it would not be appropriate to draw any conclusions about the uniformity of the dot size from photoluminescence spectra alone. It has been found, for example, that spectral linewidths of quantum dot arrays can become narrow without

Authorized licensed use limited to: IEEE Xplore. Downloaded on November 14, 2008 at 07:29 from IEEE Xplore. Restrictions apply.

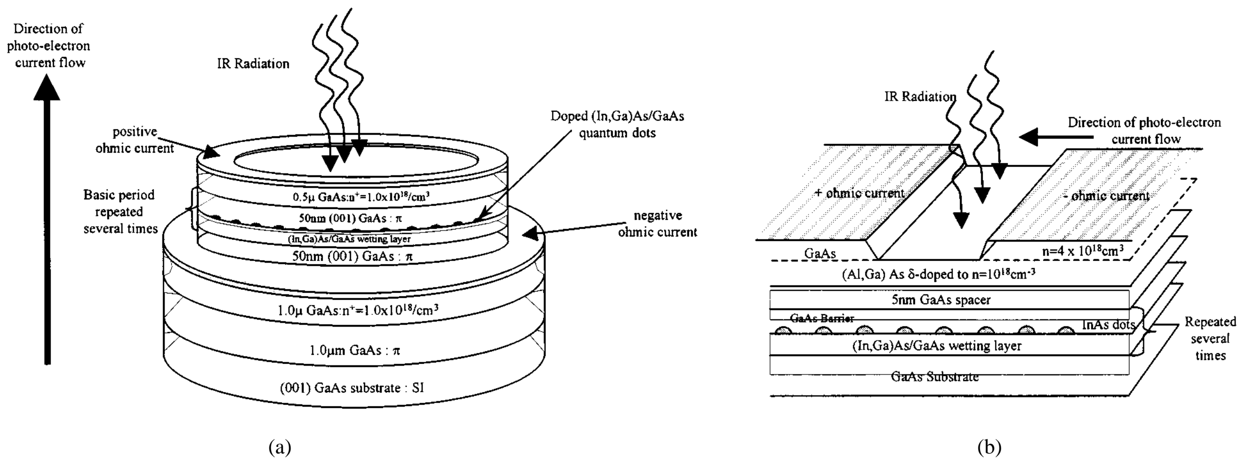

Fig. 8. Schematic diagrams of the two basic quantum-dot detector structures. Structure (a) is identical to the conventional quantum-well infrared detector structure; here, the photo-excited carriers use vertical transport through the stack of self-assembled quantum-dot layers to reach the external circuit for current conduction. In structure (b), the carriers use lateral transport similar to that in a channel of a field-effect transistor.

any obvious improvement in the uniformity of the dot sizes [as determined from AFM or transmission electron microscope (TEM) observations]. The spectral narrowing can often be attributed to either a vertical or a lateral quantum mechanical coupling between the dots [60].

V. Quantum-Dot Infrared Photodetectors

A. Structure of a Quantum-Dot Photodetector

There are two possible kinds of device structures for a quantum-dot infrared photodetector; this classification is based on the direction in which the photocarriers move. The conventional photodetector structure is shown in Fig. 8(a). The photoelectrons in this structure move along the (perpendicular) growth direction when a static electric field is applied normal to the plane of the quantum-dot layers. An alternative structure, shown in Fig. 8(b), has the photoelectrons moving laterally along the growth plane. This latter structure is believed to offer a potential for better performance because the electrons can move much more readily in a plane parallel to the dot layers than perpendicular to them. Operation of the lateral device structure at temperatures as high as 190 K has been reported in the literature [39]. Despite this advantage, however, the implementation of the lateral device structure in focal plane array applications is rather cumbersome. Because of this, we will focus our discussion here on the vertical structure.

The typical quantum-dot photodetector consists of, from the substrate up, a heavily doped n-type, 1.0-μm-GaAs bottom contact layer, followed by an infrared-sensitive active region composed of either a quantum-dot superlattice structure or a single quantum-dot layer; the active region is terminated by a top, heavily doped, n-type GaAs cap layer. The device is essentially a fancy, photosensitive resistor. We have demonstrated its operation in structures with active regions with as few as five periods of the (In,Ga)As–GaAs structure [35], and with as many as 40 periods [34]. The GaAs barrier layers in our structures typically range from about 30 to 50 nm; these are sufficiently thick that the vertical quantum-mechanical coupling between the dots can be ignored. The (In,Ga)As quantum-dot layers are doped with silicon. In our work, we have attempted, but not always succeeded, to impart only one or two electrons per dot. The reasons for wanting to have only one or two electrons per dot will become clear in a later section. Our device structures are typically grown at a substrate temperature of about 500 °C.

The device features—which are mesas of different sizes—are defined by photolithography and wet-chemical etching. The top and bottom ohmic contacts to the devices are formed from alloyed Ni–AuGe–Au.

B. Intersublevel Absorption and Photocurrent Spectra

There have been many reports on the conduction intersublevel transition energies (wavelengths) of various quantum-dot systems [61]–[73]. Two of the most widely studied dot systems for potential detector applications are the n-type (In,Ga)As–GaAs [61]–[69] and the p-type SiGe–Si systems [71]–[73]. For the (In,Ga)As–GaAs materials system, a variety of intersublevel energy differences—hence, absorption wavelengths—ranging from 30 to 120 meV have been reported [60]–[70]. This variation in transition energy is probably a result of the different dot sizes, shapes, and densities of the samples grown in the different laboratories. In order to gain information on the conduction energy levels in quantum dots, several characterization methods have been used. These include room-temperature absorption, low-temperature photocurrent absorption, photoluminescence excitation spectroscopy, and state-filling spectroscopy. Among these, the low-temperature photocurrent spectroscopy provides the most accurate and reliable measurement of the intersublevel transition energies.

Fig. 9 shows photocurrent spectra from one of our 20-period (In,Ga)As–GaAs infrared detector structures at several bias voltages. The incident light is normal to the device surface. The density of the dots (as determined from AFM observations) is about 3×10^{10} cm^{-2} in this sample. This structure is doped with silicon to give an equivalent sheet carrier density of about 1.5×10^{11} cm^{-2}; this translates into five electrons per dot. There are clearly two absorption bands in this spectrum. There is a strong peak at the wavelength of 13 μm. The spectral linewidth of this band is about 1.5 μm ($\Delta\lambda/\lambda = 11\%$). Besides the primary peak at 13 μm, we also observe a secondary

Authorized licensed use limited to: IEEE Xplore. Downloaded on November 14, 2008 at 07:29 from IEEE Xplore. Restrictions apply.

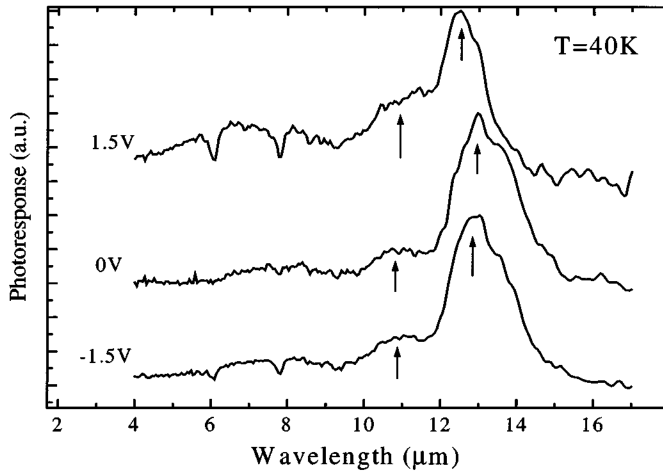

Fig. 9. Low-temperature (40 K) photocurrent spectrum of a 20-period (In,Ga)As-on-GaAs quantum-dot detector at zero bias. The peak sensitivity for this device occurs at about 13 μm.

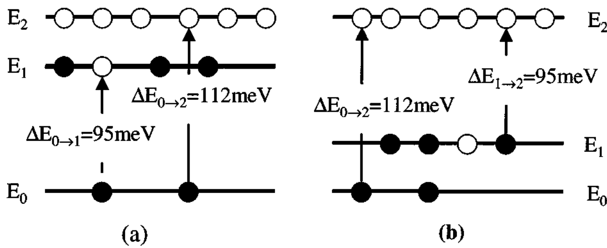

Fig. 10. A possible configuration of the electronic structure of an intersublevel quantum-dot detector.

peak at 11 μm, with a spectral width of 1.7 μm ($\Delta\lambda/\lambda = 15\%$). Note that the observed absorption bands are narrow. These spectral bands are indicative of bound-to-bound state transitions; bound-to-continuum state transitions usually exhibit relatively broad linewidths ($\Delta\lambda/\lambda > 20\%$) [4]. In Fig. 9, there is a suggestion of a weak bump around 7 μm; this bump is probably due to a bound-to-continuum transition. If we do not consider this transition, then the other observed absorption peaks suggest that we could think of the conduction band structure of the quantum dots in this sample as shown in Fig. 10.

The observation of two main absorption peaks suggests that at least three energy levels are involved in the process of intersublevel transition. There are two possible transition mechanisms: 1) electrons are excited from the ground state E_0 to the states E_1 and E_2 [shown in Fig. 10(a)], or 2) electrons are excited from the ground level E_0, and from the second confined state E_1, to the excited state E_2, as shown in Fig. 10(b). The energy spacing between these levels is as shown. The second mechanism is highly unlikely because the energy spacing between E_0 and E_1 is smaller than that between E_1 and E_2. In terms of the simplest conduction structure of the quantum dots, the permitted maximum number of electrons is two for the ground level E_0, and four for the second level E_1. Because the maximum available number of electrons per dot is five in our structure, we can reasonably assume that the level E_0 is fully occupied by two electrons. In the first case [Fig. 10 (a)], the measured energy spacing—as determined from the photocurrent spectrum in Fig. 9—between the E_0 and E_1 levels is about 95 meV, and it is 112 meV between E_0 and E_2. These energy spacings are representative of bound-to-bound state transitions.

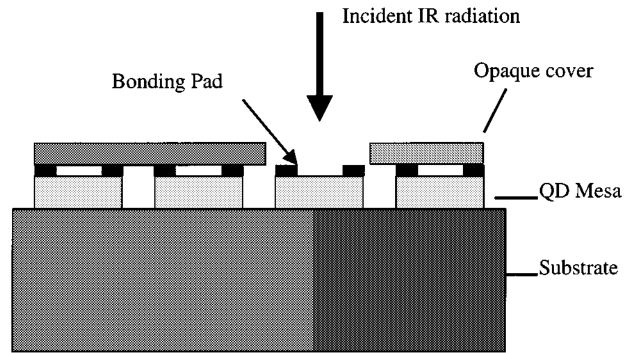

Fig. 11. Measurement scheme for characterizing infrared detectors grown on semi-insulating GaAs substrates. This arrangement minimizes the effects of light scattering and reflections from the substrate in contributing to the measured quantities.

Here, we point out that the quantum-mechanical selection rule for intersubband transitions in symmetric quantum wells, namely, $\Delta n = \text{odd}$, is not valid for quantum dots because the profile of the conduction band structure is inversion-asymmetric because of the interaction of the wetting layers and the fact that the transition matrix element from E_0 to E_2 is nonzero, as is observed in asymmetric quantum wells. In the case of the quantum dots, this is confirmed by a strong photovoltaic effect in the structures; we discuss this effect later.

C. Measurement of the Performance of Quantum-Dot Infrared Photodetectors

Before we discuss the performance of the quantum-dot detectors, we want to comment on one aspect associated with the measurement of the characteristics of normal-incidence infrared photodetectors. It is often difficult to ascertain the contribution of true normal-incidence light to the absorption process in very thin films (such as quantum wells or quantum dots) grown on semi-insulting GaAs susbtrate [74]. This is because a semi-insulting GaAs substrate does not absorb in the infrared spectral range of interest, but it can cause spurious reflections and scattering into the thin film. The reflections from the substrate and the scattering (from adjacent pixels) can contribute to the measured responsivity for normal incidence, and care should be exercised in accounting for such effects. In order to minimize the effects of scattering, an opaque glass plate was used to cover the entire array of devices, except for the single device mesa under test (as shown in Fig. 11).

D. Responsivity of Photoconductive Quantum-Dot Detectors

Fig. 12 shows a typical low-temperature (30 K) responsivity ($\Re$) for one of our five-period (In,Ga)As–GaAs quantum-dot detectors. The absorption band of this device peaks at the wavelength of 10 μm. Also shown alongside the measured responsivity is the calculated quantum efficiency ($\eta = \Re hc/e\lambda g$). There are three distinct regions of responsivity as a function of bias; these are low response region, saturation response region, and avalanche response region. At the low response re-

Authorized licensed use limited to: IEEE Xplore. Downloaded on November 14, 2008 at 07:29 from IEEE Xplore. Restrictions apply.

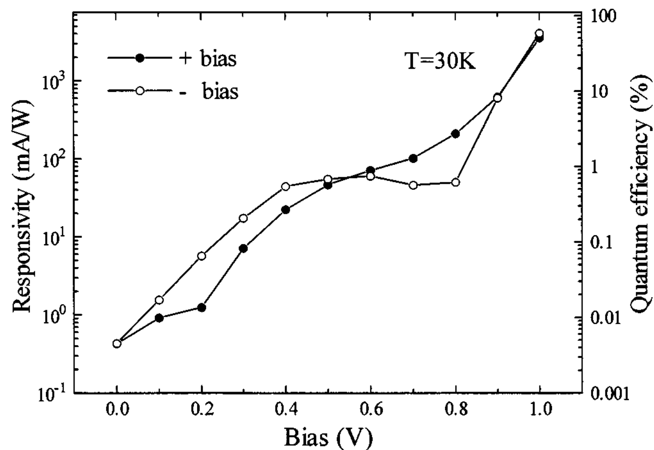

Fig. 12. Low-temperature (30 K) responsivity of a photoconductive five-period (In,Ga)As-on-GaAs quantum-dot detector; also shown is the calculated quantum efficiency.

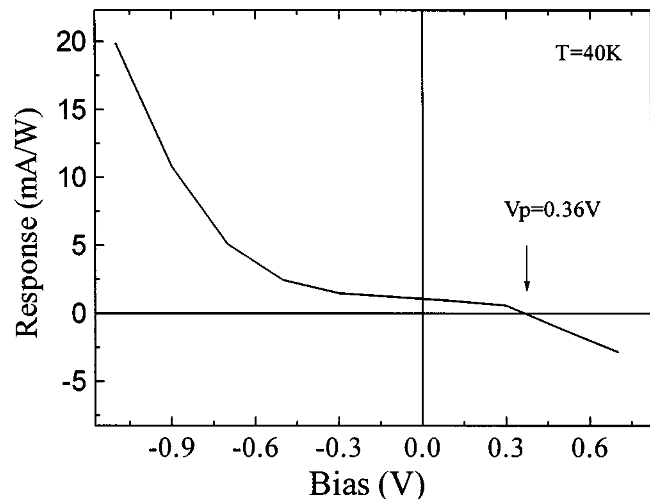

Fig. 13. Low-temperature (40 K) responsivity of a 20-period photovoltaic (In,Ga)As-on-GaAs quantum-dot detector.

gion, the measured responsivity increases linearly with bias. Note, however, that the responsivity is larger under negative bias than it is under positive bias when the voltage is less than 0.5 V (20 kV/cm). When the bias voltage is larger than 0.5 V, the responsivity is smaller under the negative bias regime. The responsivity saturation region is more pronounced under the negative bias regime than it is under positive bias. In saturation, the responsivity is between 40 and 70 mA/W. After saturation, it increases very rapidly to about 4 A/W at a bias of 4 V. The corresponding quantum efficiency is over 49%. This is suggestive of the onset of an avalanche multiplication process [4]; this process typically occurs when photoexcited electrons are subjected to very high electrical fields (in this case, around 40 kV/cm).

As stated earlier, we have also demonstrated the operation of quantum-dot infrared detectors with 20 and 40 periods of (In,Ga)As–GaAs in the sensitive superlattice region [34], [35]. The increase in the number of superlattice periods can enhance the absorption of the sensitive region, but it does not apparently improve the peak responsivity of the devices under standard operating conditions. The main reason is that the gain can decrease with an increase in the number of superlattice periods. The increase in the number of superlattice periods can provide an opportunity for the formation of deleterious dislocations. These can lead to large dark currents.

E. Photovoltaic Quantum-Dot Detectors

The photosensitive region of conventional quantum-well photodetectors is built from a basic unit comprising of a quantum-well sandwiched between two identical barriers. For the most part, the electronic structure of such an active region is symmetric about a plane of symmetry at the midpoint of the region. Most of the device characteristics for quantum-well detectors are therefore symmetric. Any pronounced asymmetry in the characteristics of such devices is usually intentionally designed into them. The most common techniques for incorporating asymmetries in quantum-well structures include grading the barriers unequally on either side of the well, sandwiching the well between barriers of unequal band gaps, or nonuniformly doping the barriers [75]–[79]. The net result of carrying out any of these actions is a built-in electrical field in the active region of the quantum-well structure. Quantum-well devices with built-in electrical fields can operate as photovoltaic detectors: in other words, no applied external bias is necessary for the device to operate.

Quantum-dot photodetectors are intrinsically photovoltaic. This property originates primarily from the geometric shape of the dots. The physical structure of the dot has no plane of symmetry perpendicular to the growth direction. This asymmetry in structure can, and does, lead to experimentally observable effects. The asymmetry can be observed, for example, from all of the responsivity characteristics of our detectors when a positive and then a negative bias is applied. Fig. 13 shows the peak responsivity for various applied bias voltages from our 20-period detector. The measured photovoltaic responsivity is about 1 mA/W (at zero bias voltage). The responsivity is zero at the bias voltage of 0.36 V. This voltage is dropped across the 20-period quantum-dot superlattice. The potential drop across each layer is therefore about 18 mV; this voltage is generally referred to as the *compensation voltage*.

As already discussed above, a photovoltaic effect, such as the one observed here, usually indicates the presence of a built-in electrical field. Because self-organized quantum dots are intrinsically asymmetric with respect to the growth plane [see Fig. 14(a)], the inherent strain distribution, and the band structure of the quantum dots will also be asymmetric. Because the wetting layers in our structures introduce a shallower potential than do the dots, an overall asymmetrical band structure is naturally formed. In addition to the asymmetric effect of the wetting layer, the dots are also asymmetric with respect to the growth plane because of their shape—which can be pyramidal or planoconvex lens-shaped, depending on the growth conditions. The shape of the dots, therefore, further increases the degree of asymmetry of the band structure of the detector layers. We schematically show, in Fig. 14(b), a version of the band structure of a quantum-dot active region along the [001] direction (from the substrate side up). Electrons in the excited state of such a structure are swept across by the built-in field, thus

Authorized licensed use limited to: IEEE Xplore. Downloaded on November 14, 2008 at 07:29 from IEEE Xplore. Restrictions apply.

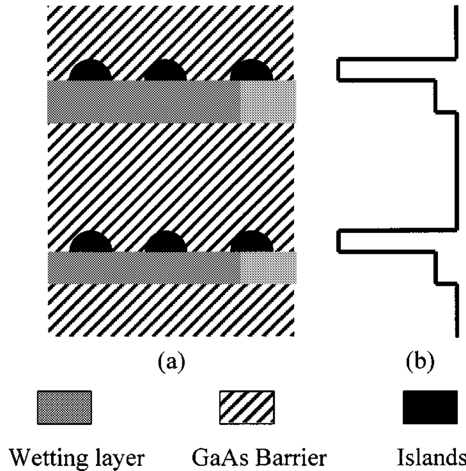

Fig. 14. Schematic diagram of stacked layers of (a) (In,Ga)As-on-GaAs quantum-dot islands; (b) the electronic structure of the conduction band of such layers.

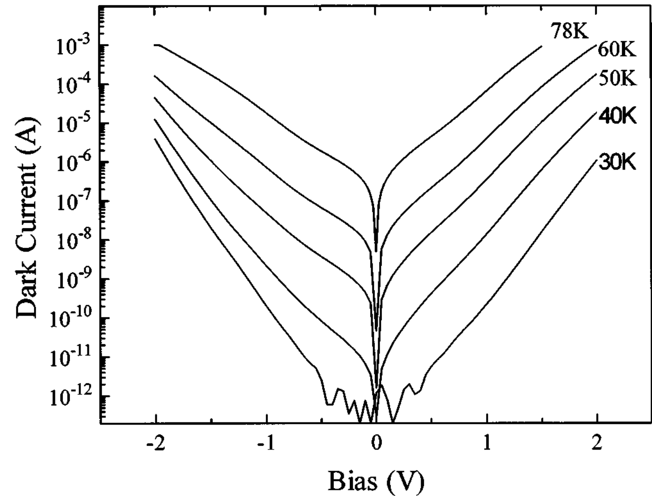

Fig. 15. The dark current-voltage characteristics of a 20-period (In,Ga)As–GaAs quantum-dot detector measured at various temperatures. Note the oscillations that manifest the effects of sequential tunneling at 30 K.

contributing to the photocurrent. Our measurements here establish the fact that the photovoltaic quantum-dot detector operates under the same principles as the photovoltaic quantum-well detector.

F. Detector Dark Current

The dark current in a photodetector is defined as the current that originates from sources other than photoexcitation. In general, the dark current in quantum-dot detectors appears to obey the same physics as that in quantum-well devices. There are three components to the dark current: 1) the thermionic component; 2) the thermally assisted tunneling component; and 3) the temperature-independent component of the current. In the thermionic component, carriers are thermally excited to continuum states above the barrier where they become part of the overall current. The thermionic component of the current depends exponentially on temperature and is expected to dominate at temperatures above 50 K. For the thermally assisted tunneling component of the current, the carriers are thermally excited into higher states below the top of well, where they can tunnel through the triangular tip of the barrier into the continuum states on the other side of the barrier. The temperature-independent component of the tunneling current refers to the contribution from tunneling of carriers between wells or dots; this component has many features of sequential resonant tunneling. Overall, no satisfactory model has yet been developed to explain the dark current in quantum-dot devices. This is largely because the band structure of quantum-dot nanostructures depends on several factors that are difficult to control experimentally at the present time.

We have measured the dark current–voltage (*I*–*V*) characteristics of the devices we have fabricated. The *I*–*V* characteristics (in the dark) for a typical 20-period (In,Ga)As–GaAs device structure are shown in Fig. 15 for various temperatures. This particular device has a peak spectral response at 13 μm at 40 K. From the characteristics in Fig. 15, we can infer that at low temperatures, the mechanism that appears to dominate the dark current is tunneling assisted. At extremely low temperatures—for example at 30 K—sequential resonant tunneling is observable. As the temperature is raised, the dark current increases exponentially with bias, indicating that the main source of the dark current is thermionic emission.

G. Detector Noise Properties and Optical Gain

We have measured the noise current, I_s, of our devices using a spectrum analyzer. From this, we are able to determine the optical gain. The noise in the photoconductive mode is dominated by the shot noise; so the noise current is

$$I_s = \sqrt{4egI_D\Delta f}$$

where
- I_D dark current;
- Δf measurement bandwidth; and
- g gain.

This equation is a specific case of Beck's [80] general formulation of the current noise in detectors. In the photovoltaic mode, the total noise is dominated by the thermal noise and the current is

$$I_{th} = \sqrt{\frac{4kT}{R_0}\Delta f}$$

where k is Boltzmann's constant and T is the absolute temperature in degrees Kelvin. The other parameters have their usual meanings. In general, the thermal noise is lower than is the shot noise, thus leading to a better noise performance figure when the detector is operated in the photovoltaic mode. Fig. 16 shows the noise performance of one of our devices at the temperatures of 40 and 78 K. The device used in these measurements is the 20-period (In,Ga)As–GaAs quantum-dot device. The dashed curves show the calculated thermal noise characteristic based on differential conductivities obtained from measured dark currents. We note that the measured noise at 40 K is limited by the external circuit noise in the range between −0.5 and 0.5 V. The measured noise at 78 K shows a reasonable trend with a decrease in the applied voltage; at zero bias, the noise is close

Authorized licensed use limited to: IEEE Xplore. Downloaded on November 14, 2008 at 07:29 from IEEE Xplore. Restrictions apply.

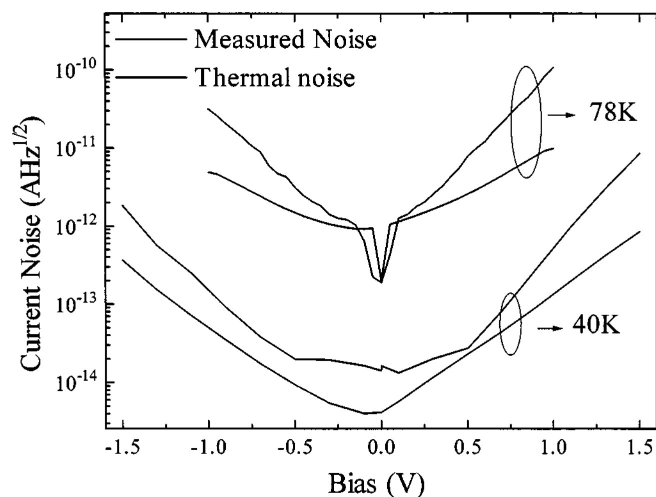

Fig. 16. The measured and calculated low-temperature (78 K) noise characteristics of a quantum-dot detector.

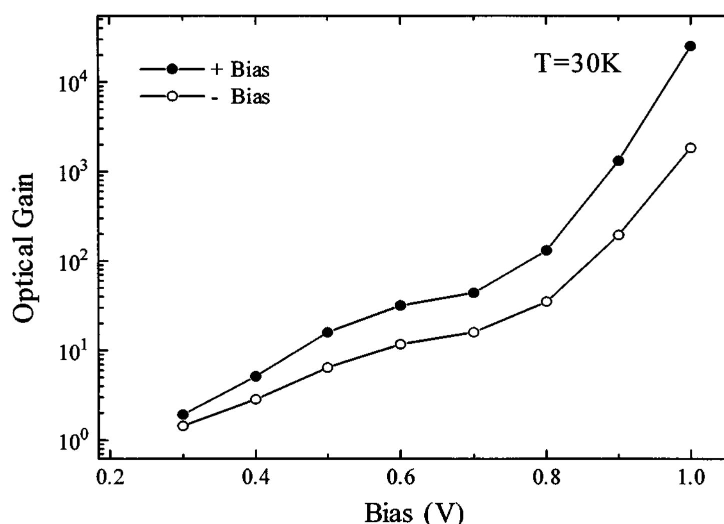

Fig. 17. The photoconductive gain of a five-period (In,Ga)As-on-GaAs quantum-dot detector for both negative and positive bias.

to the calculated thermal noise, indicating that the total noise characteristic in the photovoltaic mode is limited by the thermal noise; this, of course, is to be expected.

There is an ongoing debate on the role of phonons on the excited state lifetime of carriers in quantum dots [81]–[86]. It is speculated that the optical gain in quantum-dot detectors should be higher than in comparable quantum-well devices because of the effects of the so-called phonon bottleneck [81]. The phonon bottleneck is thought to be a consequence of the fact that strong quantum-confinement effects (at the nanometer scale) in all three dimensions produce energy sublevel separations that are much larger than a few millielectronvolts (as can be seen in our photocurrent measurements). These energy level separations are much larger than is the energy of longitudinal optical (LO) phonons. It is then predicated on this that a strongly reduced energy relaxation rate cannot be avoided—unless the energy level separation can be made comparable to the LO phonon energy. However, it is beginning to be appear that the "phonon bottleneck" may not prevent efficient energy relaxation processes in quantum dots. For example, intense photoluminescence from ground-state recombination is generally observed from the self-organized quantum dots. The data from our gain measurement also appear to support this point. The characteristics in Fig. 17 show gain as a function of bias for one of our five-period quantum-dot photodetectors. Electron transport appears to be slightly better under positive than under negative bias. In both cases, the gain increases with bias. At the positive bias of +0.5 V, the optical gain is about 20, indicating excellent electron transport. The gain is, in general, larger than that in (Al,Ga)As–GaAs quantum-well infrared detectors [4]. However, it is about the same order of magnitude as that reported for (In,Ga)As–GaAs quantum-well detectors [17]. The estimated carrier lifetime from our gain measurements is on order of several picoseconds. This estimate falls within the trend that the "phonon bottleneck" is not a problem that prevents excited carriers from relaxing into ground states in quantum dots [85], [86]. In a recent study using near- and far-field photoluminescence excitation spectroscopy of quantum dots, Toda *et al.* [86] found the existence of 2-D continuum states in a large zero-absorption region from the quasi–zero-dimensional (0-D) density of states and the 2-D wetting layer absorption edge. Within the continuum states, the carriers can relax easily inside the dots and make transitions to the ground states by a resonant emission of localized phonons.

H. Detectivity

Detectivity is a kind of a universal measure of quality for detectors. For our case, we have used the expression

$$D^* = \Re\sqrt{A\Delta f}/I_n$$

for calculating the detectivity; A is the active area of the device, $\Re$ is the responsivity, and the other parameters are as defined earlier. Fig. 18 shows the calculated D^* at 40 and 78 K from a 20-period (In,Ga)As–GaAs quantum-dot detector. The calculated low-temperature (78 K) peak detectivity is about 2×10^8 cm·Hz$^{1/2}$/W in the photovoltaic mode. This value is close to the theoretical performance limit of n-type photoconductive quantum-well detectors at the same wavelength [4], and is comparable to present-day photovoltaic quantum-well detectors. At the temperature of 40 K, the highest D^* is about 7×10^9 cm·Hz$^{1/2}$/W at the bias of 0.85 V; the corresponding responsivity is 23 mA/W. It is evident from these data and what has been reported in the literature that the performance of quantum-dot detectors still lags that of quantum-well detectors at identical wavelengths (for example, the detectivity of a typical GaAs–(Al,Ga)As quantum-well detector at the temperature of 77 K is about 7×10^{10} cm·Hz$^{1/2}$/W; see [4], for example). We venture to give an analysis of the reasons why this is so in the next section.

VI. Discussion

A good photodetector should have high responsivity and low dark current. In the section on intersublevel absorption and photocurrent spectra, we showed that the conduction band structure of present-day quantum-dot infrared photodetectors consists of

Authorized licensed use limited to: IEEE Xplore. Downloaded on November 14, 2008 at 07:29 from IEEE Xplore. Restrictions apply.

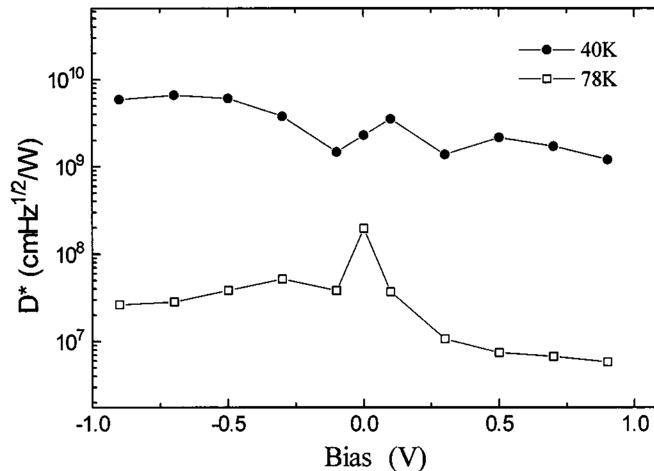

Fig. 18. The calculated detectivity (D^{*}) of a 20-period (In,Ga)As–GaAs quantum-dot detector at the operating temperatures of 40 and 78 K.

at least three bound states and a continuum state above the barrier. If we assume that the electron configuration of a quantum dot is $2n$ for the energy level n, then the maximum number of electrons for the ground state is two; it is four for first excited state, and six for the second excited state. The oscillator strength is largest for the intersublevel transition between the energy levels E_0 and E_1. The strongest absorption therefore occurs between a fully occupied ground state and the first excited state as long as at least two unoccupied slots are in it. If there are more than six electrons per dot (and state occupation is sequential), then the transitions between the states E_0 and E_1 will be inhibited. The transitions $E_0 \rightarrow E_2$ and $E_0 \rightarrow E_c$, although allowed, are weak and therefore do not lead to much sensitivity. And so the corresponding responsivity will be low. From the point of view of the dark current, the number of electrons in the excited states (under no illumination) should be zero; all electrons should be in the fully occupied ground state. These are the ideal conditions to strive for to achieve a high-performance quantum-dot infrared detector.

It has been experimentally established by Levine *et al.* [4] that quantum-well infrared photodetectors that use bound-to-continuum state transitions tend to exhibit much higher responsivities than do any other type of quantum-well detector. This is generally thought to be because of the excellent hot-electron transport properties in the continuum states. Because most quantum-dot infrared detectors reported to date are based on bound-to-bound state transitions, where the photoexcited electrons must tunnel through a barrier to form the photocurrent, it is not surprising that the responsivity of the quantum-dot detectors is rather low. Consider, for example, that in Fig. 12, the calculated quantum efficiency of our devices is only 1%, even in the saturation region. In order to enhance the responsivity of these detectors, it may be essential to modify the band structure of the quantum dots so that the devices operate on the basis of bound-to-continuum state transitions or bound-to-quasi-continuum state transitions. Another key issue is the fact that the dot density so far has been limited to about $1 \times 10^{11}/\text{cm}^2$ per layer, with a wide distribution in dot sizes. These factors, we believe, are responsible for the observed low responsivity from the reported devices.

The dark current is associated with doping. Because of the small density-of-states in a quantum dot, the excited states are easily filled. This can, and does, result in excessive dark currents. Careful filling of the states is therefore essential. As an example, if the ideal state-filling conditions discussed earlier are not met, a dopant concentration that results in three electrons per dot in a device structure will lead to a larger dark current than a concentration that results in only two electrons per dot. This condition imposes a rather stringent requirement on the control of dopant atoms necessary for a quantum-dot detector. Although the doping process is uniform with respect to a growth plane, the random distribution of the self-formed quantum dots and the variation in their size, may result in some dots being overdoped or underdoped. In the case of overdoping, the carriers may begin to occupy excited states, resulting in unwanted dark currents.

The basic challenges in fabricating high-performance quantum-dot detectors are rooted in the synthesis of the dots. At this time, not enough is known on how to precisely control the self-organization process so that the desired size, shape, and density of the dots can be obtained. As a consequence, the electronic structure of the dots is difficult to modify and optimize. This is another reason for the rather low responsivity of the quantum-dot photodetectors. Some interim approaches are being applied for modifying and controlling the electronic structure of the dots. One such approach is to control the strain field around the dots. This has been successful for extending the wavelength of interband emission from InAs-on-GaAs quantum dots to 1.3–1.5 μm [87]–[91]. This approach, in theory, can also be used for controlling the intersublevel transition energy. Another more tractable method is to control the quantum-mechanical coupling among the dots. This is simply accomplished by either changing the areal density of the dots or by decreasing the barrier thickness among multiple, vertically stacked quantum-dot layers. Because the density of dots in a typical structure can range from 10^9 to $10^{11}/\text{cm}^2$, this approach appears to be the simplest to implement. The effects of quantum-mechanical coupling of dots on the conduction band energy structure are significant enough that they can be used to change the intersublevel transition energy. We have recently demonstrated that the intersubevel absorption wavelength can be tuned from 15 to 10 μm [92] in this manner. We believe that the future of the quantum-dot detector is intertwined with the control of the physical and, hence, the electronic structure of the dot. More explicitly, much remains to be done in developing approaches to 1) control the size of the dot; 2) increase the density; 3) uniformly dope the dots with the desired number of dopant atoms; and 4) regulate the spatial location of the dots. Progress toward this end continues to be made [93], [94]. In time, we believe that optoelectronic and electronic devices whose operation and characteristics depend on careful and precise nanostructure engineering will be as common place as most quantum-well devices in use today.

Summary

We have described the progress and the challenges that remain in the development of high-performance quantum-dot detectors. At this stage of their development, these type of detectors are still clearly inferior to the related quantum-well infrared photodetectors. However, because of their potential

Authorized licensed use limited to: IEEE Xplore. Downloaded on November 14, 2008 at 07:29 from IEEE Xplore. Restrictions apply.

theoretical promise, quantum-dot detectors are likely to emerge as an alternative to QWIP's. The key advantages that the quantum-dot nanostructures potentially offer include their ability to sense normal-incidence radiation, ease of the device fabrication process, flexibility in the tunability of the desired wavelength of operation, and an intrinsic photovoltaic capability.

ACKNOWLEDGMENT

The authors gratefully acknowledge contributions to this work from S. Kennerly of the U.S. Army Research Laboratory in Adelphi, MD. They also thank F. Capasso and C. Gmachl for providing us with Fig. 2.

REFERENCES

[1] S. Nakamura, M. Senoh, S. Nagahama, N. Iwasa, and T. Yamada, "Continuous-wave operation of InGaN/GaN/AlGaN-based laser diodes grown on GaN substrates," *Appl. Phys. Lett.*, vol. 72, pp. 2014–2016, 1998.

[2] H. Morkoç, "Wurzite GaN-based heterostructures by molecular beam epitaxy," *IEEE J. Select. Topics Quantum Electron.*, vol. 4, pp. 537–549, 1998.

[3] J. Faist, F. Capasso, D. L. Sivco, C. Sirtori, A. L. Hutchinson, and A. Y. Cho, "Quantum cascade laser," *Science*, vol. 263, pp. 553–555, 1994.

[4] B. F. Levine, "Quantum-well infrared photodetectors," *J. Appl. Phys.*, vol. 74, pp. R1–R81, 1993.

[5] R. Eisberg and R. Resnick, *Quantum Physics of Atoms, Molecules, Solids, Nuclei, and Particles*. New York: Wiley, 1974, pp. 14–24.

[6] M. Arias, M. Zandian, J. G. Pasko, J. Bajaj, L. J. Kozlowski, W. E. Tennant, and R. E. DeWames, "MBE HgCdTe IRFPA flexible manufacturing," in *Proc. SPIE*, vol. 2274, 1994, pp. 2–16.

[7] G. Destefanis, P. Audebert, E. Mottin, and P. Rambaud, "High performance LWIR 256 × 256 HgCdTe focal plane array operating at 88 K," in *Proc. SPIE*, vol. 3061, 1997, pp. 111–116.

[8] P. Tribolet, J. P. Chatard, P. Costa, and A. Manissadjian, "Progress in HgCdTe homojunction infrared detectors," *J. Cryst. Growth*, vol. 184–185, pp. 1262–1271, 1998.

[9] R. A. Soref, "Extrinsic IR photoconductivity of Si doped with B, Al, Ga, P, As, or Sb," *J. Appl. Phys.*, vol. 38, pp. 5201–5208, 1967.

[10] L. West and S. Eglash, "First observation of an extremely large-dipole infrared transition within the conduction band of a GaAs quantum well," *Appl. Phys. Lett.*, vol. 46, pp. 1156–1158, 1985.

[11] B. Levine, K. Choi, C. Bethea, J. Walker, and R. Malik, "New 10 μm infrared detector using intersubband absorption in resonant tunneling GaAlAs superlattices," *Appl. Phys. Lett.*, vol. 50, pp. 1092–1094, 1987.

[12] S. D. Gunapala and K. M. S. V. Bandara, "Recent developments in quantum-well infrared photodetectors," in *Homojunction and Quantum-Well Infrared Detectors*, M. H. Francombe and J. L. Vossen, Eds. San Diego, CA: Academic, 1995, vol. 21, pp. 113–237.

[13] S. Li, "Recent progress in quantum well infrared photodetectors and focal plane arrays for IR imaging applications," *Mater. Chem. Phys.*, vol. 50, pp. 188–194, 1997.

[14] P. Bois, E. Costard, J. Y. Duboz, and J. Nagle, "Technology of multiple quantum well infrared detectors," in *Proc. SPIE*, vol. 3061, 1997, pp. 764–771.

[15] A. Rogalski, "Comparison of the performance of quantum well and conventional bulk infrared photodectors," *Infrared Phys. Technol.*, vol. 38, pp. 295–310, 1997.

[16] S. D. Gunapala, S. V. Bandara, J. K. Liu, W. Hong, M. Sundaram, R. Carralejo, C. A. Shott, P. D. Maker, and R. E. Miller, "Long-wavelength 640 × 484 GaAs/Al_xGa_{1-x}As quantum well infrared photodetector focal plane array camera," in *Proc. SPIE*, vol. 3061, 1997, pp. 722–727.

[17] S. D. Gunapala, K. M. S. V. Bandara, B. F. Levine, G. Sarusi, J. S. Park, T. L. Pike, and J. K. Liu, "High performance InGaAs/GaAs quantum well infrared photo detectors," *Appl. Phys. Lett.*, vol. 64, pp. 3431–3433, 1994.

[18] G. Hasnain, B. F. Levine, C. G. Bethea, R. A. Logan, J. Walker, and R. J. Malik, "GaAs/AlGaAs multiquanturn well infrared detector arrays using etched gratings," *Appl. Phys. Lett.*, vol. 54, pp. 2515–2517, 1989.

[19] G. Sarusi, B. F. Levine, S. J. Pearton, K. M. S. V. Bandara, and R. E. Leibenguth, "Optimization of two dimensional gratings for very long wavelength quantum well infrared photodetectors," *J. Appl. Phys.*, vol. 76, pp. 4989–4994, 1994.

[20] ——, "Improved performance of quantum well infrared photodetectors using random scattering optical coupling," *Appl. Phys. Lett.*, vol. 64, pp. 960–962, 1994.

[21] C. J. Chen, K. K. Choi, W. H. Chang, and D. C. Tsui, "Corrugated quantum well infrared photodetectors with polyimide planarization for detector array applications," *IEEE Trans. Electron Devices*, vol. 45, pp. 1431–1437, 1998.

[22] L. Esaki and H. Sakaki, "New photoconductor," *IBM Tech. Disc. Bull.*, vol. 20, pp. 2456–2457, 1977.

[23] Y. Arakawa and H. Sakaki, "Multidimensional quantum well laser and temperature dependence of its threshold current," *Appl. Phys. Lett.*, vol. 40, pp. 939–941, 1982.

[24] L. Goldstein, F. Glas, J. Y. Marzin, M. N. Charasse, and G. LeRoux, "Growth by molecular beam epitaxy and characterization of InAs/GaAs strained-layer superlattices," *Appl. Phys. Lett.*, vol. 47, pp. 1099–1101, 1984.

[25] S. Guha, A. Madhukar, and K. C. Rajkumar, "Onset of incoherency and defect introduction in the initial stages of molecular beam epitaxial growth of highly strained InGaAs on GaAs (100)," *Appl. Phys. Lett.*, vol. 57, pp. 2110–2112, 1990.

[26] G. J. Whaley and P. I. Cohen, "Relaxation of strained InGaAs during molecular beam epitaxy," *Appl. Phys. Lett.*, vol. 57, pp. 144–146, 1990.

[27] D. Leonard, M. Krishnamurthy, C. M. Reaves, S. P. Denbaars, and P. M. Petroff, "Direct formation of quantum-sized dots from uniform coherent islands of InGaAs on GaAs surface," *Appl. Phys. Lett.*, vol. 63, pp. 3203–3205, 1993.

[28] F. Heinrichsdorff, A. Krost, M. Grundmann, D. Bimberg, A. Kosogov, and P. Werner, "Self-organization processes of InGaAs/GaAs quantum dots grown by metalorganic chemical vapor deposition," *Appl. Phys. Lett.*, vol. 68, pp. 3284–3286, 1996.

[29] D. L. Huffaker, G. Park, Z. Zou, O. B. Shchekin, and D. G. Deppe, "1.3 μm room-temperature GaAs-based quantum-dot laser," *Appl. Phys. Lett.*, vol. 73, pp. 2564–2566, 1998.

[30] D. Bimberg, M. Grundmann, and N. N. Ledentsov, "Growth, spectroscopy and laser application of self-ordered III–V quantum dots," *Mater. Res. Soc. Bull.*, vol. 23, pp. 31–34, 1998.

[31] H. Saito, K. Nishi, I. Ogura, S. Sugou, and Y. Sugimoto, "Room-temperature lasing operation of a quantum-dot vertical-cavity surface-emitting laser," *Appl. Phys. Lett.*, vol. 69, pp. 3140–3142, 1996.

[32] F. Schäfer, J. P. Reithmaier, and A. Forchel, "High-performance GaInAs/GaAs quantum-dot lasers based on a single active layer," *Appl. Phys. Lett.*, vol. 74, pp. 2915–2917, 1999.

[33] D. Pan, E. Towe, and S. Kennerly, "Normal-incidence intersubband (In, Ga)As/GaAs quantum dot infrared photodetectors," *Appl. Phys. Lett.*, vol. 73, pp. 1937–1939, 1998.

[34] D. Pan and E. Towe, "Conduction intersubband (In,Ga)As/GaAs quantum dot infrared photodetectors," *Electron. Lett.*, vol. 34, pp. 1883–1884, 1998.

[35] D. Pan, E. Towe, and S. Kennerly, "A five-period normal-incidence intersubband (In, Ga)As/GaAs quantum dot infrared photodetectors," *Appl. Phys. Lett.*, vol. 75, pp. 2719–2721, 1999.

[36] J. Phillips, K. Kamath, and P. Bhattacharya, "Far-infrared photoconductivity in self-organized InAs quantum dots," *Appl. Phys. Lett.*, vol. 72, pp. 2020–2022, 1998.

[37] S. Kim, H. Mohseni, M. Erdtmann, E. Michel, C. Jelen, and M. Razeghi, "Growth and characterization of InGaAs/InGaP quantum dots for midinfrared photo conductive detector," *Appl. Phys. Lett.*, vol. 73, pp. 963–965, 1998.

[38] S. Xu, S. J. Chua, T. Mei, X. C. Wang, X. H. Zhang, G. Karunasiri, W. J. Fan, C. H. Wang, J. Jiang, S. Wang, and X. G. Xie, "Characteristics of InGaAs quantum dot infrared photodetectors," *Appl. Phys. Lett.*, vol. 73, pp. 3153–3155, 1998.

[39] S.-W. Lee, K. Hirakawa, and Y. Shimada, "Bound-to-continuum intersubband photoconductivity of self-assembled InAs quantum dots in modulation-doped heterostructures," *Appl. Phys. Lett.*, vol. 75, pp. 1428–1430, 1999.

[40] I. N. Stranski and L. Krastanow, "Zur theorie der orientierten ausscheidung von lonenkristallen aufeinander," *Sitzungsberichte d. Akad . d. Wissenschaften in Wein, Abt. IIb*, vol. 146, pp. 797–810, 1937.

[41] S. Fafard, Z. Wasilewski, J. McCaffrey, S. Raymond, and S. Charbonneau, "InAs self-assembled quantum dots on InP by molecular beam epitaxy," *Appl. Phys. Lett.*, vol. 68, pp. 991–993, 1996.

Authorized licensed use limited to: IEEE Xplore. Downloaded on November 14, 2008 at 07:29 from IEEE Xplore. Restrictions apply.

[42] V. M. Ustinov, E. R. Weber, S. Ruvimov, Z. Liliental-Weber, A. E. Zhukov, A. Yu. Egorov, A. R. Kovsh, A. F. Tsatsul'nikov, and P. S. Kop'ev, "Effect of matrix on InAs self-organized quantum dots on InP substrate," *Appl. Phys. Lett.*, vol. 72, pp. 362–364, 1998.

[43] E. Alphandéry, R. J. Nicholas, N. J. Mason, B. Zhang, P. Möck, and G. R. Booker, "Self-assembled InSb quantum dots grown on GaSb: A photoluminescence, magnetoluminescence, and atomic force microscopy study," *Appl. Phys. Lett.*, vol. 74, pp. 2041–2043, 1999.

[44] K. K. Linder, J. Phillips, O. Qasaimeh, X. F. Liu, S. Krishna, and P. Bhattacharya, "Self-organized $In_{0.4}Ga_{0.6}As$ quantum-dot lasers grown on Si substrates," *Appl. Phys. Lett.*, vol. 74, pp. 1355–1357, 1999.

[45] D. J. Eaglesham and M. Cerullo, "Dislocation-free Stranski–Krastanow growth of Ge on Si(100)," *Phys. Rev. Lett.*, vol. 64, pp. 1943–1946, 1990.

[46] S. P. Guo, H. Ohno, A. Shen, F. Matsukura, and Y. Ohno, "InAs self-organized quantum dashes grown on GaAs (211)B," *Appl. Phys. Lett.*, vol. 70, pp. 2738–2740, 1997.

[47] A. Polimeni, M. Henini, A. Patane, L. Eaves, and P. C. Main, "Optical properties and device applications of (InGa)As self-assembles quantum dots grown on (311)B GaAs substrates," *Appl. Phys. Lett.*, vol. 73, pp. 1415–1417, 1999.

[48] K. Akahane, T. Kawamura, K. Okino, H. Koyama, S. Lan, Y. Okada, and M. Kawabe, "Highly packed InGaAs quantum dots on GaAs(311)B," *Appl. Phys. Lett.*, vol. 73, pp. 3411–3413, 1998.

[49] A. Konkar, A. Madhukar, and P. Chen, "Stress-engineered spatially selective self-assembly of strained InAs quantum dots on nonplanar patterned GaAs(001) substrates," *Appl. Phys. Lett.*, vol. 72, pp. 220–222, 1998.

[50] R. Zhang, R. Tsui, K. Shiralagi, D. Convey, and H. Goronkin, "Selective formation and alignment of InAs quantum dots over mesa stripes along the [011] and [001] directions on GaAs (100) substrates," *Appl. Phys. Lett.*, vol. 73, pp. 505–507, 1998.

[51] Y. H. Xie, S. B. Samavedam, M. Bulsara, T. A. Langdo, and E. A. Fitzgerald, "Relaxed template for fabricating regularly distributed quantum dot arrays," *Appl. Phys. Lett*, vol. 71, pp. 3567–3568, 1997.

[52] D. Pan, J. Xu, and E. Towe, "Self-organization of (In,Ga)As/GaAs quantum dots on relaxed (In,Ga)As films," *Appl. Phys. Lett.*, vol. 73, pp. 2164–2166, 1998.

[53] G. Soloman, J. A. Trezza, and J. S. Harris Jr., "Effects of monolayer coverage, flux ratio, and growth rate on the island density of InAs islands on GaAs," *Appl. Phys. Lett.*, vol. 66, pp. 3161–3163, 1995.

[54] M. Grundmann, J. Christen, N. N. Ledentsov, J. Bohrer, D. Bimberg, S. S. Ruvimov, P. Werner, U. Richter, U. Gosele, J. Heydenreich, V. M. Ustinov, A. Y. Egorov, A. E. Zhukov, P. S. Kop'ev, and Z. I. Alferov, "Ultranarrow luminescence lines from single quantum dots," *Phys. Rev. Lett.*, vol. 74, pp. 4043–4046, 1995.

[55] H. Lee, R. Lowe-Webb, W. Yang, and P. C. Sercel, "Determination of the shape of self-organized InAs/GaAs quantum dots by reflection high energy electron diffraction," *Appl. Phys. Lett.*, vol. 72, pp. 812–814, 1998.

[56] H. Saito, K. Nishi, and S. Sugou, "Shape transition of InAs quantum dots by growth at high temperature," *Appl. Phys. Lett.*, vol. 74, pp. 1224–1226, 1999.

[57] S. Takagi, "A dynamical theory of diffraction for a distorted crystal," *J. Phys. Soc. Jpn.*, vol. 26, pp. 1239–1253, 1969.

[58] A. Krost, F. Heinrichsdorff, D. Bimberg, A. Darhuber, and G. Bauer, "High-resolution X-ray diffraction of self-organized InGaAs/GaAs quantum dot structures," *Appl. Phys. Lett.*, vol. 68, pp. 785–787, 1996.

[59] A. Krost, J. Bläsing, F. Heinrichsdorff, and D. Bimberg, "In enrichment in (In,Ga)As/GaAs quantum dots studied by high-resolution X-ray diffraction and pole figure analysis," *Appl. Phys. Lett.*, vol. 75, pp. 2957–2959, 1999.

[60] G. S. Solomon, J. A. Trezza, A. F. Marshall, and J. S. Harris, "Vertically aligned and electronically coupled growth induced InAs islands in GaAs," *Phys. Rev. Lett.*, vol. 76, pp. 952–955, 1996.

[61] H. Drexler, D. Leonard, W. Hansen, J. P. Kotthaus, and P. M. Petroff, "Spectroscopy of quantum levels in charge-tunable InGaAs quantum dots," *Phys. Rev. Lett.*, vol. 73, pp. 2252–2255, 1994.

[62] D. Pan, Y. P. Zeng, M. Y. Kong, J. Wu, Y. Q. Zhu, H. Zhang, and J. M. Li, "Normal incidence infrared absorption from InGaAs/GaAs quantum dot superlattice," *Electron. Lett.*, vol. 32, pp. 1726–1727, 1996.

[63] D. Pan, E. Towe, and S. Kennerly, "Strong normal-incidence infrared absorption and photo-current spectra from highly uniform (In,Ga)As/GaAs quantum dot structures," *Electron. Lett.*, vol. 34, pp. 1019–1020, 1998.

[64] J. Phillips, K. Kamath, X. Zhou, N. Chervela, and P. Bhattacharya, "Photoluminescence and far-infrared absorption in Si-doped self-organized InAs quantum dots," *Appl. Phys. Lett.*, vol. 71, pp. 2079–2081, 1997.

[65] K. W. Berryman, S. A. Lyon, and M. Segev, "Mid-infrared photoconductivity in InAs quantum dots," *Appl. Phys. Lett.*, vol. 70, pp. 1861–2255, 1997.

[66] S. Maimon, E. Finkman, G. Bahir, S. E. Schacham, J. M. Garcia, and P. M. Petroff, "Intersublevel transitions in InAs/GaAs quantum dots infrared photodetectors," *Appl. Phys. Lett.*, vol. 73, pp. 2003–2005, 1998.

[67] S. Xu, S. J. Chua, T. Mei, X. C. Wang, X. H. Zhang, G. Karunasiri, W. J. Fan, C. H. Wang, J. Jiang, S. Wang, and X. G. Xie, "Polarization dependence of intraband absorption in self-organized quantum dots," *Appl. Phys. Lett.*, vol. 73, pp. 1997–1999, 1998.

[68] S. Sauvage, P. Boucaud, F. H. Julien, J. M. Gerard, and J. Y. Marzin, "Infrared spectroscopy of intraband transitions in self-organized InAs/GaAs quantum dots," *J. Appl. Phys.*, vol. 82, pp. 3396–3401, 1997.

[69] Q. D. Zhuang, J. M. Li, H. X. Li, Y. P. Zeng, L. Pan, Y. H. Chen, M. Y. Kong, and L. Y. Lin, "Intraband absorption in the 8–12 μm band from Si-doped vertically aligned InGaAs/GaAs quantum-dot superlattice," *Appl. Phys. Lett.*, vol. 73, pp. 3706–3708, 1998.

[70] A. Weber, O. Gauthier-Lafaye, F. H. Julien, J. Brault, M. Gendry, Y. Désieres, and T. Benyattou, "Strong normal-incidence infrared absorption in self-organized InAs/InAlAs quantum dots grown on (001) InP," *Appl. Phys. Lett.*, vol. 74, pp. 413–415, 1999.

[71] J. L. Liu, W. G. Wu, A. Balandin, G. Jin, Y. H. Luo, S. G. Thomas, Y. Lu, and K. L. Wang, "Observation of inter-sub-level transitions in modulation-doped Ge quantum dots," *Appl. Phys. Lett.*, vol. 75, pp. 1745–1747, 1999.

[72] P. Boucaud, V. Le. Thanh, S. Sauvage, D. Débarre, and D. Bouchier, "Intraband absorption in Ge/Si self-assembled quantum dots," *Appl. Phys. Lett.*, vol. 74, pp. 401–403, 1999.

[73] J. L. Liu, W. G. Wu, A. Balandin, G. L. Jin, and K. L. Wang, "Intersubband absorption in boron-doped multiple Ge quantum dots," *Appl. Phys. Lett.*, vol. 74, pp. 185–187, 1999.

[74] H. C. Liu, M. Buchanan, and Z. R. Wasilewski, "How good is the polarization selection rule for intersubband transitions?," *Appl. Phys. Lett.*, vol. 72, pp. 1682–1684, 1998.

[75] H. Schneider, P. Koidl, C. Schonbein, S. Ehret, E. C. Larkins, and G. Bihlmann, "Capture dynamics and infrared response in photovoltaic quantum well intersubband photodetectors," *Superlattices and Microstruc.*, vol. 19, pp. 347–364, 1996.

[76] K. W. Goosen, S. A. Lyon, and K. Alavi, "Photovoltaic qauntum well detectors," *Appl. Phys. Lett.*, vol. 52, pp. 1701–1703, 1988.

[77] A. Kastalsky, T. Duffield, S. J. Allen, and J. Harbison, "Photovoltaic detection of infrared light in a GaAs/AlGaAs superlattice," *Appl. Phys. Lett.*, vol. 52, pp. 1320–1322, 1988.

[78] C. Schonbein, H. Schneider, G. Bihlmann, K. Schwarz, and P. Koidl, "A 10μm AlGaAs/GaAs intersubband photodetector operating at zero bias voltage," *Appl. Phys. Lett.*, vol. 68, pp. 973–975, 1996.

[79] H. Schneider, C. Schonbein, M. Walther, K. Schwarz, and P. Koidl, "Photovoltaic quantum well infrared photodetectors: Four zone scheme," *Appl. Phys. Lett.*, vol. 71, pp. 246–268, 1997.

[80] W. A. Beck, "Photoconductive gain and generation-recombination noise in multiple-quantum-well infrared detectors," *Appl. Phys. Lett.*, vol. 63, pp. 3589–3591, 1993.

[81] H. Benisty, C. M. Sotomayor-Torres, and C. Weisbuch, "Intrinsic mechanism for the poor luminescence properties of quantum-box systems," *Phys. Rev.*, vol. B 44, pp. 10 945–10 948, 1991.

[82] M. Sugawara, K. Mukai, and H. Shoji, "Effect of phonon bottleneck on quantum-dot laser performance," *Appl. Phys. Lett.*, vol. 71, pp. 2791–2793, 1997.

[83] V. Uskov, Y. Boucher, and J. Le Bihan, "Theory of a self-assembled quantum-dot semiconductor laser with Auger carrier capture: Quantum efficiency and nonlinear gain," *Appl. Phys. Lett.*, vol. 73, pp. 1499–1501, 1998.

[84] V. Uskov, J. McInerney, F. Adler, H. Schweizer, and M. H. Pilkuhn, "Auger carrier capture kinetics in self-assembled quantum dot structures," *Appl. Phys. Lett.*, vol. 72, pp. 58–60, 1998.

[85] Y. Toda, O. Moriwaki, M. Nishioka, and Y. Arakwa, "Efficient carrier relaxation mechanism in InGaAs/GaAs self-formed quantum dots based on the existence of continuum states," *Phys. Rev. Lett.*, vol. 82, pp. 4114–4117, 1999.

[86] R. Ferreira and G. Bastard, "Phononassisted capture and intradot Auger relaxation in quantum dots," *Appl. Phys. Lett.*, vol. 74, pp. 2818–2820, 1999.

[87] H. Saito, K. Nishi, and S. Sugou, "Influence of GaAs capping on the optical properties of InGaAs/GaAs surface quantum dots with 1.5 μm emission," *Appl. Phys. Lett.*, vol. 73, pp. 2742–2744, 1998.

Authorized licensed use limited to: IEEE Xplore. Downloaded on November 14, 2008 at 07:29 from IEEE Xplore. Restrictions apply.

[88] K. Nishi, H. Saito, S. Sugou, and J.-S. Lee, "A narrow photoluminescence linewidth of 21 meV at 1.35 μm from strain-reduced InAs quantum dots covered by $In_{0.2}Ga_{0.8}As$ grown on GaAs substrates," *Appl. Phys. Lett.*, vol. 74, pp. 1111–1113, 1999.
[89] R. Heitz, N. N. Ledentsov, D. Bimberg, A. Y. Egorov, M. V. Maximov, V. M. Ustinov, A. E. Zhukov, Zh. I. Alferov, I. P. Soshnikov, N. D. Zakharov, P. Werner, and U. Gösele, "Optical properties of InAs quantum dots in a Si matrix," *Appl. Phys. Lett.*, vol. 74, pp. 1701–1703, 1999.
[90] V. M. Ustinov, N. A. Maleev, A. E. Zhukov, A. R. Kovsh, A. Y. Egorov, A. V. Lunev, B. V. Volovik, I. L. Krestnikov, Yu. G. Musikhin, N. A. Bert, P. S. Kop'ev, Zh. I. Alferov, N. N. Ledentsov, and D. Bimberg, "InAs/InGaAs quantum dot structures on GaAs substrates emitting at 1.3 μm," *Appl. Phys. Lett.*, vol. 74, pp. 2815–2817, 1999.
[91] J. Bloch, J. Shah, W. S. Hobson, J. Lopata, and S. N. G. Chu, "Room-temperature 1.3 μm emission from InAs quantum dots grown by metal organic chemical vapor deposition," *Appl. Phys. Lett.*, vol. 75, pp. 2199–2201, 1999.
[92] D. Pan, E. Towe, S. Kennerly, and M. Y. Kong, "Tunning of conduction inter-sublevel absorption wavelengths in (In,Ga)As/GaAs quantum dot nanostructures," *Appl. Phys. Lett.*, vol. 76, pp. 3537–3539, 2000.
[93] I. Mukhametzhanov, R. Heitz, J. Zeng, P. Chen, and A. Madhukar, "Independent manipulation of density and size of stress-driven self-assembled quantum dots," *Appl. Phys. Lett.*, vol. 73, pp. 1841–1843, 1998.
[94] T. Ishikawa, S. Kohmoto, and K. Asakawa, "Site control of self-organized InAs dots on GaAs substrates by in situ electron-beam lithography and molecular-beam epitaxy," *Appl. Phys. Lett.*, vol. 73, pp. 1712–1714, 1998.

Elias Towe, photograph and biography not available at the time of publication.

Dong Pan, photograph and biography not available at the time of publication.

Authorized licensed use limited to: IEEE Xplore. Downloaded on November 14, 2008 at 07:29 from IEEE Xplore. Restrictions apply.